Nanoscale Advances

ROYAL SOCIETY OF CHEMISTRY

PAPER

View Article Online
View Journal | View Issue

Cite this: *Nanoscale Adv.*, 2020, **2**, 1904

Modulation of protein–graphene oxide interactions with varying degrees of oxidation†

Shahid A. Malik,[ab] Zinia Mohanta,[bc] Chandan Srivastava[d] and Hanudatta S. Atreya *[ab]

The degree of oxidation of graphene oxide (GO) has been shown to be important for its toxicity and drug-loading efficiency. However, the effect of its variations on GO–protein interaction remains unclear. Here, we evaluate the effect of the different oxidation degrees of GO on its interaction with human ubiquitin (8.6 kDa) using solution state nuclear magnetic resonance (NMR) spectroscopy in combination with other biophysical techniques. Our findings show that the interaction between the protein and the different GO samples is weak and electrostatic in nature. It involves fast dynamic exchange of the protein molecules from the surface of the GO. As the oxidation degree of the GO increases, the extent of the interaction with the protein changes. The interaction of the protein with GO can thus be modulated by tuning the degree of oxidation. This study opens up new avenues to design appropriate graphenic materials for use in various biomedical fields such as drug delivery, biomedical devices and imaging.

Received 28th December 2019
Accepted 22nd March 2020

DOI: 10.1039/c9na00807a

rsc.li/nanoscale-advances

Introduction

Graphene and graphenic materials have attracted attention owing to their intriguing properties[1–5] and applications in various fields.[6–9] The chemical modification of graphene yielding amphiphilic sheet-like GO molecules,[10] characterized by the presence of a high density of oxygen in the form of hydrophilic functional moieties such carboxylic acids, carbonyls, alcohols and epoxides,[11] is believed to modulate its compatibility in biological systems.[12] Owing to the rich oxygenic surface,[12] large surface area:volume ratio,[13] surface enhanced properties[14] and presence of hydrophobic sp^2 and sp^3 carbon on its sheet-like structure,[13] GO has been considered for different biomedical applications such as biosensing,[15,16] drug delivery,[17] bioimaging,[18] photothermal therapies,[19] tissue engineering,[20] cell growth and cell differentiation[21] and various biomedical devices.[22]

In general, any biomedical application of GO would involve its interaction with various biomolecules such as nucleic acids,[23] lipids[24] and proteins.[25] The GO surface interacts with various functional groups present on the proteins. The extent of these interactions is expected to depend upon the surface charge, surface energy and hydrophobicity of GO.[26] In the case of proteins, a 'protein corona'[27] is formed which may significantly affect not only the protein structure and function but also the biological characteristics of GO.[28–30] The formation of the protein corona on the surface affects the fate of the designed nanomaterials.[31,32] Thus, a comprehensive study of the effect of surface modifications of GO on its interaction with proteins is required for understanding and improving its biomedical efficacy.[12]

GO–protein interactions have been studied, using techniques such as Circular Dichroism (CD), fluorescence, UV-Vis spectroscopy, and Fourier transform Infra-Red spectroscopy (FTIR).[30,33,34] Using NMR spectroscopy, information about the dynamics of the protein and its individual residues can be obtained across a varying range of time scales.[35] This feature renders NMR a powerful spectroscopic technique for probing structural and dynamic perturbations in the protein backbone upon its interaction with GO.[25]

In the present work, using NMR spectroscopy in combination with other techniques such as isothermal titration calorimetry (ITC), zeta potential (ζ) measurements, FTIR spectroscopy, X-ray diffraction (XRD), X-ray photoelectron spectroscopy (XPS), CD spectroscopy, Atomic Force Microscopy (AFM) and Raman spectroscopy, we have studied the residue specific interaction of a globular protein human ubiquitin with GO prepared with different oxidation degrees.[36]

We have chosen human ubiquitin as the model globular protein in the present study because it is found in almost all eukaryotes and is an important regulatory protein involved in the ubiquitin proteasome pathway. Its structure comprises both

[a]*Department of Solid State and Structural Chemistry Unit, Indian Institute of Science, Bangalore-560012, India. E-mail: hsatreya@iisc.ac.in*

[b]*Nuclear Magnetic Resonance Research Centre, Indian Institute of Science, Bangalore-560012, India*

[c]*Centre for Bio Systems Science and Engineering, Indian Institute of Science, Bangalore-560012, India*

[d]*Department of Materials Engineering, Indian Institute of Science, Bangalore-560012, India*

† Electronic supplementary information (ESI) available. See DOI: 10.1039/c9na00807a

alpha helices and beta strands, thereby serving as an important example for exploring the mechanism of the interaction of GO with structured proteins.[25]

Experimental

Materials and methods

Purification of ubiquitin. For NMR studies, the following procedure was adopted to purify the uniformly ^{15}N labelled protein. The plasmid containing the gene for human ubiquitin was transformed into *E. coli* BL21 (DE3) cells. A few bacterial colonies were inoculated in 10 ml culture medium and were grown overnight at 37 °C. The 10 ml culture medium was pelleted down at 4000 rpm and the pellet was re-suspended in M9 minimal medium supplemented with $^{15}NH_4Cl$ (1 g per litre) and D-glucose (4 g per litre) as the source of nitrogen and carbon, respectively. The other supplements of the minimal medium include a 100× vitamin mixture, $CaCl_2$ (500 μM) and $MgCl_2$ (1 mM). When the O.D.$_{(600)}$ of the bacterial culture reached ~0.6, the culture was induced with a final concentration of 1 mM IPTG (isopropyl- β-D-1-thiogalactopyranoside) at 37 °C for 5 hours and the cells were harvested by centrifugation at 4000 rpm followed by re-suspension of the pellet in 50 mM acetate buffer (supplemented with 5 mM EDTA, pH 5). The protein was released from the cells by sonication of the pellet and, after centrifugation at 1000 rpm for 40 minutes, the supernatant was loaded onto a cation exchange SP sepharose column pre-equilibrated with acetate buffer at 4 °C, and a salt gradient (0–1 M NaCl in sodium acetate buffer at pH 5) was used to elute the protein from the column. The protein concentration was estimated using the absorbance measurement at 280 nm (the molar extinction coefficient of ubiquitin is 1490 M^{-1} cm^{-1}).

For non-NMR studies, the unlabelled protein was purified from Luria Broth (LB) in place of a minimal medium following an identical purification procedure as that described above.

Synthesis of GO with varying oxidation degrees. The synthesis of the GO samples used in this study has been reported previously[36] and is depicted in the schematic below (Fig. 1). The samples have been prepared using a two-step methodology, where the graphite powder was first ball milled for *X* hours ($X = 0, 30, 80, 100$) to introduce defects and then each ball milled graphite sample was oxidized using Tour's method to obtain the corresponding graphene oxide, G_*X*. Hence, the nomenclature of the samples used is G_0, G_30, G_80, and G_100, with G_0 being the graphene oxide prepared from un-milled graphite.

Step – I: Planetary ball milling. Planetary ball milling is a process where a powder mixture is placed in a ball-mill and then subjected to high energy collisions with stainless-steel balls. The powders are repeatedly deformed, fractured and welded during the process. The ball mill system constitutes one plate (turn disc) and two or four bowls. The plate and bowls rotate in opposite directions to each other in antagonistic synchronization. The powder mixture and milling balls are subjected to centrifugal forces, which are created due to the rotation of the bowl around its own axis and plate along its own axis. The microstructure and morphology of the powder

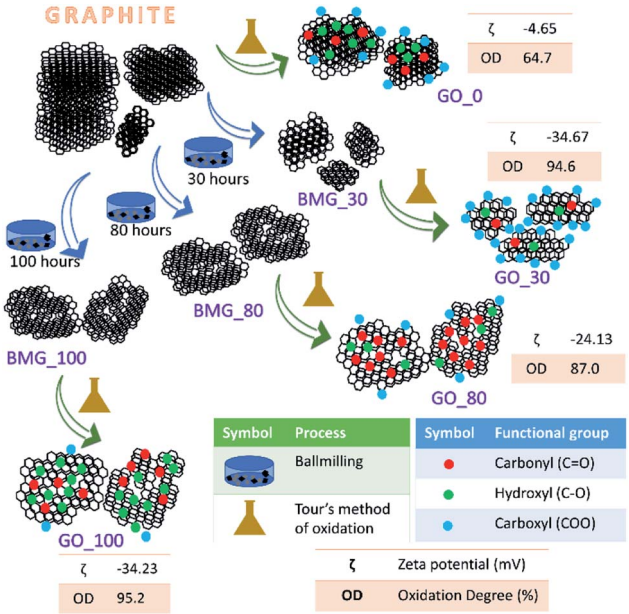

Fig. 1 Schematic representation of the synthesis of various GO samples. For each GO sample the number of ball milling hours (*X* hours), zeta potential (ζ) and percentage of the degree of oxidation (OD%) are also provided. Here BMG_*X* refers to ball milled graphite for *X* hours.

changes due to the repeated welding, fracture, and rewelding. In wet ball milling, the powder mixture is dispersed in a liquid medium. Ball milling of graphite causes exfoliation of the graphite and extended ball milling causes introduction of defects in the graphite lattice. Ball milling of the graphitic samples was performed using hexane as the solvent. Hexane was used as it has a very low boiling point (68 °C) and the solvent could be evaporated easily to procure ball milled graphite for use in the next step. The ball milling conditions are as follows: plate speed: 300 rpm, bowl speed: 700 rpm and each cycle consists of 15 minutes OFF and 8 minutes ON time (Fig. S1 in the ESI†).

Step – II: Tour's method of oxidation. 1 g of ball milled graphite and 6 g of $KMnO_4$ were mixed in a beaker. 120 ml of sulphuric acid was taken in a beaker and placed in an ice bath. To attain a proportion of 9 : 1, orthophosphoric acid with a total amount of 14 ml was added to it. Both the acids were mixed with the help of a glass rod. Then the beaker containing the mixture of graphite–$KMnO_4$ was placed in the ice bath and the acid solution was poured in the mixture immediately. Adding the solution slowly would result in a highly exothermic reaction. The reaction mixture was constantly stirred with a glass rod to obtain a suspension. A stirring bar was added to the reaction solution which was placed on a hot plate magnetic stirrer to obtain a consistent mixture. The reaction mixture was then continuously stirred for 12 hours at 45 °C. The reaction mixture was slowly poured into another beaker containing 140 ml of DI ice and stirred until the ice melted completely. This was followed by addition of 10 ml of H_2O_2 to the final mixture. The mixture turned chrome yellow. Once the mixture cooled down,

200 ml of DI water was added and was allowed to decant for 2 days. The sediment was procured and washed using DI water thrice and with ethanol twice. Later it was dried to obtain the GO powder.

During the process of synthesis (the ball milling step) of GO samples, the mechanical introduction of defects leads to a decrease in the sp^2 carbon content and introduction of oxygenic functional moieties (during the oxidation step). The overall sp^2/sp^3 ratio of the GO falls as the number of ball milling hours increases and the oxidation state increases (Table S1 in the ESI†).

Characterization of GO with varying oxidation degrees and their protein conjugates. Validation of the formation of GO was performed using Raman Spectroscopy, FTIR Spectroscopy, XRD, Solid-state Nuclear Magnetic Resonance (ss-NMR) Spectroscopy and X-ray Photoelectron Spectroscopy (XPS). From the obtained signatures of the samples from the above-mentioned studies, the formation of GO was confirmed.

Raman Spectroscopy. A LabRam HR with a 532 nm laser was used for acquiring Raman spectra. The range for spectrum acquisition was from 1000 to 3000 cm^{-1}.

FTIR spectroscopy. The presence of functional moieties in the as-synthesized GO samples was authenticated by using a PerkinElmer Frontier FT-NIR/MIR spectrometer for qualitative analysis.

XRD. A JEOL Xpert Pro PANanalytical JDX-8030 diffractometer (Cu K-alpha radiation, $\lambda = 0.1542$ nm) was used for XRD study and acquiring the d-spacing of the samples. In the XRD spectra, as shown in Fig. S3 in the ESI† (intensity plotted against 2θ), the 2θ positions of the peaks correspond to GO as reported in previous literature. There is an observable shift in the peaks towards the right. By using Bragg's law, $d = \lambda/(2 \sin \theta)$ (d is the d-spacing or interlayer spacing, λ is the X-ray wavelength and θ is the diffraction angle), the d-spacings for G_0, G_30, G_80 and G_100 were calculated (Table S1 in the ESI†).

ss-NMR spectroscopy and XPS. An ECXII JEOL 400 MHz with a 4 mm probe was used for ss-NMR spectroscopy. A 13C single pulse experiment, with delay (d1): 5 s, number of scans (ns): 8K, and a spinning speed of 10 kHz, was performed for all the GO samples. However in the ss-NMR spectra, as shown in Fig. S3 in the ESI,† expanded graphite was observed for G_0, suggesting complete oxidation of other GO samples and complete exfoliation of graphite (hence no peak in the XRD spectra). Hence, we considered the intensities of peaks present in the ss-NMR spectrum of G_0 for calculation of percentage of oxidation degree (OD%). Analysis of elemental composition was carried out using a Kratos X-ray Photoelectron Spectrometer with an Al-K-α X-ray source having an excitation energy of 1486.6 eV. The deconvolution of the high resolution C 1s spectrum was performed to obtain the relative content of nonaromatic and aromatic carbon in each GO sample and then the oxygen content was calculated. In our XRD studies, only peaks for GO were present as shown in Fig. S3 in the ESI.†

ζ measurements. The electrostatic properties of the different samples of GO were estimated by zeta potential measurements using a Nanozetasizer machine (Brookhaven Zeta PALS) with a final concentration of 50 $\mu g\ ml^{-1}$ for each GO sample.

ITC. ITC experiments were conducted using a VP-ITC calorimeter from MicroCal. About 0.5 mg ml^{-1} of each GO sample was taken in a 2 ml cell and 50 μM human ubiquitin was taken in a titration syringe. Both GO and human ubiquitin were prepared in 50 mM phosphate buffer (supplemented with 150 mM NaCl) at pH 6.0. The titration experiments were performed at 25 °C with thirty injections each of 10 μl of the protein. The stirring speed during the titration was 394 rpm. The data were analysed using MicroCal Origin software.

CD spectroscopy. All CD spectra were recorded using a Jasco J-815 CD spectrometer scanning from a wavelength of 180 nm to 350 nm in continuous scanning mode with a scanning speed of 100 nm min^{-1} and bandwidth of 2 nm. Free and conjugated forms of the protein with different GO samples were prepared in 50 mM phosphate buffer at a pH of 6.

AFM. The AFM images were acquired using an NX-10 AFM (Park Systems) system in non-contact mode. Dilute solutions of the GO samples were prepared and drop dried on silicon wafers. Then, the samples were washed carefully with Milli-Q water to remove the aggregates and then dried in a desiccator. An Al back coated Si probe (ACTA, App Nano Inc, USA) was used; it had a resonant frequency of 300 kHz and a nominal spring constant of 40 nm^{-1}. A scan size of 2 $\mu m \times 2\ \mu m$ was used with a scan rate of 0.8 Hz. All the images were processed using XEI software.

Solution state NMR spectroscopy. All NMR spectra were acquired at a temperature of 298 K on a Bruker Avance-III NMR spectrometer equipped with a triple resonance probe (cryogenically cooled) operating at a ^1H resonance frequency of 800 MHz. 2,2-dimethyl-2-silapentane-5-sulfonate (DSS) was used for chemical shift calibration, 0 ppm for protons, while ^{15}N-chemical shifts were calibrated indirectly. The experimental time for each 2D [^{15}N, ^1H] HSQC spectrum was 20 minutes with the respective offset frequencies for ^1H and ^{15}N set at 4.7 ppm and 118 ppm and the sweep widths taken as 10 ppm and 38 ppm for direct and indirect dimensions, respectively. All NMR data were processed using Topspin 3.2 software and analysed using Sparky.

Results

The terms oxidation level and degree of oxidation have been used interchangeably for expressing the extent of oxidation in graphene oxide. However, the two parameters are different and hence have to be used precisely while corroborating a hypothesis to avoid ambiguity. The oxidation level, determined using the O/C ratio gives the oxygen content of the graphite oxide and considers the stoichiometric ratio of the functional groups, that is, it provides information about the amount of oxygen present with respect to the carbon content. The degree of oxidation or oxidation degree (OD) of GO on the other hand is the amount of carbon that is oxidized. The calculation of OD takes two import factors into consideration, the aromatic and non-aromatic carbon ratio and the amount of graphite that undergoes complete oxidation. Pertaining to our study, we have considered degree of oxidation as the chemical property of interest. The

degree of oxidation for the four different types of GO prepared is indicated in Fig. 1.

The AFM results show that all the GO samples exhibited poly dispersive distribution; distinct differences could be observed. G_0 had a sheet thickness of about 19 nm indicating that the GO prepared was multi-layered. Another interesting observation was that G_30 consisted of much smaller particles and the layer thickness was about 3 nm. This type of distribution has been explained in a previously reported work from our group. G_80 and G_100 show uniform sheet structures with each sheet having a thickness of around 3 nm (Fig. S6 in the ESI†).

First, the quantification of the defect density of each GO sample was carried out by obtaining the ratio of I_D and I_G bands in the Raman spectra (Fig. S2 in the ESI†) which reveals that the defects introduced during ball milling can help in obtaining GO samples with varying degrees of oxidation and surface charges owing to the presence of different functional moieties (−COOH, –C═O, –COR, *etc.*) on the surface of the GO as reflected in the FTIR spectra (Fig. S2 in the ESI†) and Solid-state NMR spectra (Fig. S3 in the ESI†) of various GO samples.

On deconvoluting the Raman spectra of GO, we observed distinguishable peaks at 1350, 1532 and 1598 cm^{-1} (Fig. S2†). The peak at 1350 cm^{-1} arises from the disorder induced mode, A_{1g}. The Raman bands at 1532 and 1598 cm^{-1} are a combination of A_{1g}, E_{1g} and E_{2g} vibration modes. The peak at 1598 cm^{-1} is assigned to the G band. The peak at 1532 cm^{-1} can be attributed to amorphous carbon.

A broad and wide peak was observed in all the FTIR spectra (Fig. S2†) of GO samples at 3185 cm^{-1} which is ascribed to O–H stretching vibrations and is due to the presence of –OH functional moieties and intercalated water. Intense peaks at 1730, 1419 and 1041 cm^{-1} are peaks of ketone, carboxylic and epoxy groups. The FTIR spectra of the synthesized GO samples exhibiting the characteristic peaks of GO for each sample confirm the presence of oxygen containing functional moieties from successful formation of GO in each case.

To understand the nature of carbons and the contribution of sp^2 and oxidized states of carbon, the high resolution C 1s scans were obtained through XPS. The notable humps at 292 eV were considered to be because of the π–π* transitions (HOMO–LUMO), characteristic satellite peaks arising from carbon in aromatic rings. The XPS spectra were deconvoluted for sp^2 (at ∼285 eV), C–O (at ∼286.7 eV), C═O (at ∼287.9 eV), COO (at ∼290.3 eV) and π–π* (at ∼292 eV). The deconvolution of each C 1s spectrum is shown in Fig. S4 in the ESI.†

The oxygen content was quantified using the O/C ratio obtained using the relation:

$$O/C = ((2 \times I_{(COO)}) + (1 \times I_{(C-O)}) + (1 \times I_{(C=O)}))/ (I_{(C=C)} + I_{(COO)} + I_{(C-O)} + I_{(C=O)})$$

where, I_{COO}, I_{C-O}, $I_{C=O}$, and $I_{C=C}$ correspond to the intensities of the peaks corresponding to carboxyl, hydroxyl, carbonyl groups and aromatic carbon, respectively, from deconvolution of high resolution C 1s scans obtained by XPS (Table S1 in the ESI†).

The percentage of the oxidation degree (OD%), Table S1 in the ESI,† is calculated using the percentage of aromatic carbon and non-aromatic carbon, calculated from XPS data (Fig. S4 in the ESI†) and the intensities of the GO and graphite peaks in the XRD pattern of GO (as shown in Fig. S3 in the ESI†) using the following relation:

$$I_{(non\text{-}aromatic)}/(I_{aromatic} + I_{(non\text{-}aromatic)}) \times I_{GO}/(I_{GO} + I_{graphite}) \times 100$$

Quantitatively, the extent of the interaction of protein with the various synthesized GO samples was studied by ITC by measuring the dissociation constant (K_d) of the binding as shown in Fig. 2. The values of the dissociation constant (K_d) for ubiquitin with different GO samples having varying oxidation degrees fall in the micro molar range (Table 1); thus a weak electrostatic interaction is expected. This implies that ubiquitin interacts weakly with the different GO samples, indicating dynamic association–dissociation as discussed below. It should be noted that we could not obtain the saturation point in the interaction of ubiquitin with G_30 (Fig. 2) at the defined concentration of the protein (50 μM) and the number of

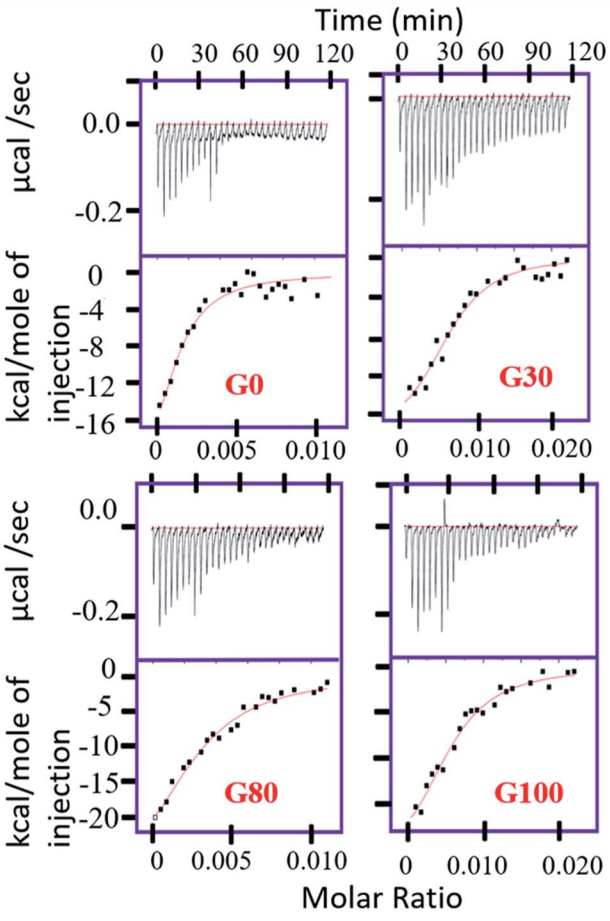

Fig. 2 ITC studies of different GO samples with human ubiquitin at 25 °C.

Table 1 List of the various thermodynamic parameters derived by ITC for interaction of different GO samples with human ubiquitin

	K_d (μM)	ΔH (cal mol^{-1})	ΔS
G_0	1.4 ± 0.8	$-3.2 \times 10^4 \pm 1.2 \times 10^4$	−81.14
G_30	1.3 ± 0.35	$-2.05 \times 10^4 \pm 2933$	−41.66
G_80	2.5 ± 0.75	$-3.55 \times 10^4 \pm 9265$	−93.5
G_100	1.9 ± 0.4	$-3.04 \times 10^4 \pm 1.36 \times 10^4$	−75.64

injections (30 injections total) of protein as used for the other GO samples.

The CD spectra of the ubiquitin conjugates with GO samples having varying degrees of oxidation and surface chemistry show a decreasing ellipticity, which is because of the decrease in the population of free ubiquitin upon interaction with various GO samples. We did not observe any appreciable shift in the CD spectra of the ubiquitin upon conjugation with different GO samples (Fig. S5 in the ESI†), implying that the the secondary structure of the protein is retained upon interaction with various GO samples.

NMR studies of the ubiquitin-GO interaction

To characterize and quantify the dynamic aspects of the interaction of ubiquitin with various types of GO at the residue level, we recorded 2D [^{15}N, ^{1}H] Heteronuclear Single Quantum Coherence (HSQC) NMR spectra and amide proton relaxation times T_2 ($^{1}H_N$) of the protein sample in the presence and absence of each GO sample at pH 6.[25,37,38] In a 2D [^{15}N, ^{1}H] HSQC NMR spectrum each cross-peak corresponds to a directly bonded ^{1}H–^{15}N spin pair (with the exception of proline residues); thus the individual behaviour of each residue of ubiquitin can be probed using the intensity of its own cross-peak belonging to that amide bond.[37]

Two types of titrations were performed, forward titration and reverse titration.[25,37,39,40] In the former (forward) titration, from a stock of 1 mg ml^{-1}, successive amounts of a particular GO sample (20 μl, 30 μl, 40 μl, 50 μl and 60 μl corresponding to a final concentration of each GO sample of 38.4 μg ml^{-1}, 56.6 μg ml^{-1}, 74.1 μg ml^{-1}, 90.9 μg ml^{-1} and 107.1 μg ml^{-1} after considering the dilution of the whole volume) were added to 500 μl of the uniformly ^{15}N-labeled ubiquitin (100 μM) dissolved in 50 mM phosphate buffer supplemented with 150 mM NaCl and 5% $^{2}H_2O$ at pH 6. This is referred to as 'forward titration'.

In the second type of titration (referred to as 'reverse titration'), ^{15}N-labeled ubiquitin (stock concentration 500 μM) was gradually added to 500 μl of each GO (70 μg ml^{-1}) taken in an NMR tube. The protein was added in increments of 10 μl, 20 μl, 30 μl, 40 μl, 50 μl, 60 μl and 70 μl corresponding to a final concentration of the protein of ~9.4 μM, 18.5 μM, 27.3 μM, 35.7 μM, 44.0 μM, 51.7 μM and 59.3 μM. This titration helps to obtain the approximate amounts of protein loaded onto each GO surface and hence the effect of varying the surface chemistry of the GOs on the protein loading tendency can be probed as described below.

Forward titration: addition of GO to ubiquitin

Fig. 3a and b, respectively, show an overlay of the spectra of the free ubiquitin (blue) with that in the presence of the G_0 sample (red) and the plot of normalized 2D [^{15}N, ^{1}H] HSQC peak intensities (with respect to the free protein) in the presence of indicated amounts of G_0, at a pH of 6.0 and 298 K. Fig. 3c–h depict similar interactions for G_30, G_80 and G_100.

Two observations can be made by looking at the spectra. First, no appreciable chemical shift perturbations of the peaks were observed upon addition of different GOs, suggesting that the protein retains its structural integrity upon interaction with different GOs.

Second, for a number of peaks the intensities are appreciably reduced with complete broadening of some of the cross peaks upon successive addition of GO, suggesting the potential

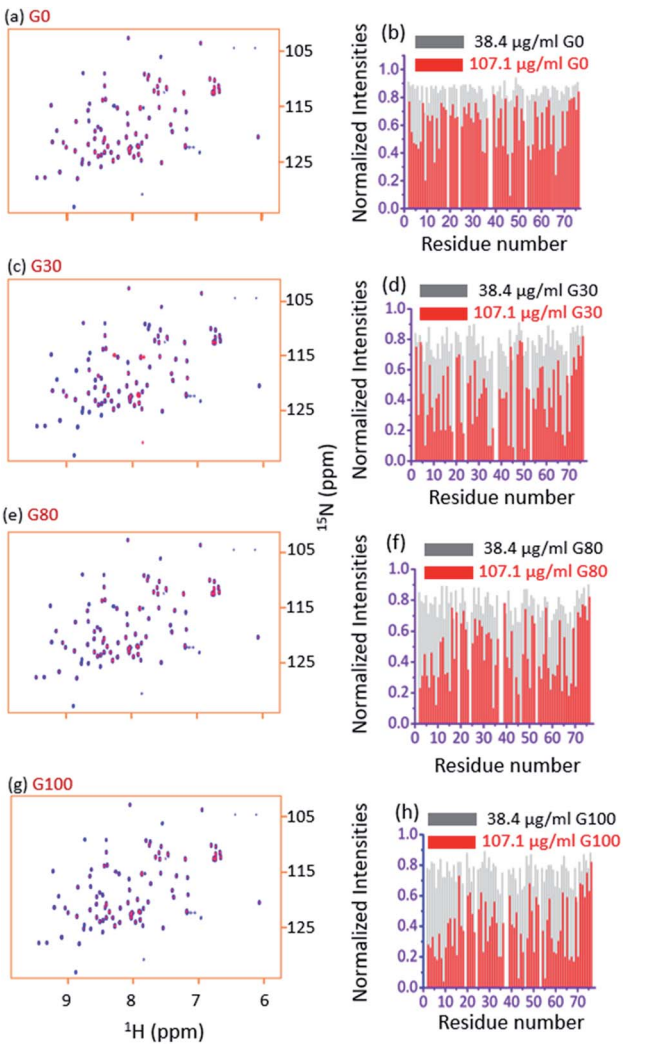

Fig. 3 (a and b) The overlay of the 2D [^{15}N, ^{1}H] HSQC spectra of free ubiquitin (blue) with that in the presence of 107.1 μg ml^{-1} of G_0 (red) and the plot of normalized 2D [^{15}N, ^{1}H] HSQC peak intensities (with respect to the free protein) in the presence of the indicated amounts of G_0, at a pH of 6.0 and 298 K, respectively. Figures (c), (d), (e), (f), (g), and (h) represent the same for G_30, G-80 and G_100, respectively.

residues of the protein that are involved in the interaction with the GO surface.

If the protein interacts strongly with the oppositely charged functional groups on the surface of the GO, there will be a significant fall in the T_2 values of the protein because of the large molecular weight of the protein-GO conjugate formed (slow exchange). The larger the molecular weight of the conjugate, the smaller the T_2 values. The residues which interact directly with the GO surface will be completely broadened out upon addition of the GO. Thus, the observed signals, if any, in the spectrum will have arisen from the free (unbound) protein molecules in the solution. In such a case, further addition of the GO should not vary the T_2 (^1H_N) values of the unbound protein significantly. In the other scenario, if the increasing amounts of the GO lead to a decrease in the T_2 (^1H_N) values of the protein, it implies that the free (unbound) protein molecules undergo a "fast exchange" with the protein molecules bound to the surface of the GO ($\Delta R_2 \ll k_{ex}$). This observed decrease in the T_2 (^1H_N) values of the protein is a consequence of the increase in the relative population of the bound protein molecules as the titration proceeds, hence resulting in a population weighted average of the observed R_2 (^1H_N) as:

$$R_{2(obs)} = 1/T_{2(obs)} = p_{free} \times 1/T_{2free} + p_{bound} \times 1/T_{2bound}$$

where p_{free}, $1/T_{2free}$ and p_{bound}, $1/T_{2bound}$ are the relative populations and $1/T_2$ (^1H_N) values of free and bound ubiquitin, respectively. In order to measure the amide proton transverse relaxation times T_2 (^1H_N) of the free and the bound form of ubiquitin, we used a two-point HSQC method, a modified version of the pulse sequence described previously,[41] which was used for the measurement of the paramagnetic relaxation enhancement (Γ) in proteins. The modification involves the introduction of an additional delay during the first INEPT and acquisition of two spectra (two-point HSQC), each with an additional delay time (16 ms in the first (referred to as "with delay spectrum" and 20 μs in the second (referred to as "without delay spectrum"))), while keeping all the parameters constant.[25,37]

The residue specific exponential decay of the signals of amide protons (^1H_N) as observed in a 2D [^{15}N, ^1H] HSQC NMR experiment due to the transverse relaxation of spins can be written as:

$$I = \exp(-\tau/T_2(^1H_N))$$

Here 'τ' represents the period during which the amide protons (^1H_N) are in the transverse plane. Next, we acquired two 2D [^{15}N, ^1H] HSQC spectra such that all other parameters are kept constant, except for the two additional delay times introduced, as a result of which the NMR signal shows an extra decay.

The ratio of the NMR signal intensities of the two HSQC spectra acquired with (τ_2) and without delay (τ_1) will be:

$$I_{\text{with delay}}/I_{\text{without delay}} = \exp(-(\tau_2 - \tau_1)/T_2(^1H_N))$$

where $\tau_2 - \tau_1 \approx 16$ ms is the difference between the two additionally inserted delays. The above equation can be rearranged to give:

$$T_2(^1H_N) = (\tau_2 - \tau_1)/\ln(I_{\text{without delay}}/I_{\text{with delay}})$$

Thus, a residue specific plot of T_2 (^1H_N) can be obtained using the ratios of peak intensities in the two spectra acquired with two delays. Further, if the ratios of peak intensities relative to those in the free protein are considered, the effect on the intensity from $^3J_{HNHA}$ during the additional delay period is removed. The measured values of amide proton transverse relaxation times (T_2 (^1H_N)) are provided in the ESI† and the normalized relative T_2 (^1H_N) values of ubiquitin upon titration with the various GO samples at varying concentrations are plotted as shown in Fig. 4.

As can be seen in Fig. 4a–d, for all the residues the observed T_2 (^1H_N) of ubiquitin falls as we gradually titrate with a particular GO sample. This trend is observed for all GOs. This further shows that the fraction of the bound form of ubiquitin (f_{bound}) gradually increases upon gradual addition of the GO to the protein solution, and hence a fast exchange of protein on the surface of the GO is implied. As the oxidation degree of the GO increases, the number of residues broadening out also increases, confirming that the GO with a higher oxidation degree binds more protein molecules. The residues that undergo the highest reduction (*i.e.*, ≥75%) in T_2 (^1H_N) values are:

For G_0: T9, A46, T66.

For G_30: K6, T7, G10, I13, L15, V17, E18, T22, I23, K27, K29, E34, G35, I36, L43, F45, A46, L50, N60, E64, L67, H68.

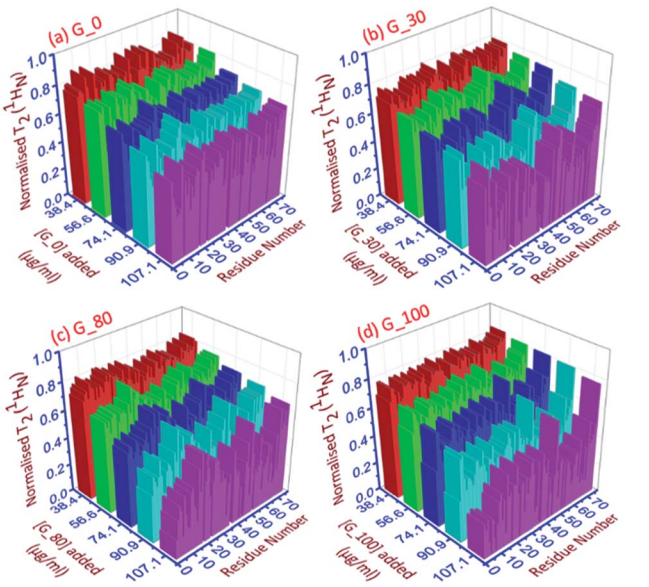

Fig. 4 The 3D representation of the relative normalized T_2 (^1H_N) values of each residue for each ubiquitin-GO conjugate at different indicated additions of (a) G_0, (b) G_30, (c) G_80 and (d) G_100.

For G_80: Q2, K6, T9, G10, L15, E34, L43, I44, F45, A46, L50, Y59, E64, L67, H68, V70.

For G_100: Q2, I3, V5, K6, T7, L8, T9, G10, I13, L15, K27, E34, G35, L43, F45, A46, L50, T55, Y59, N60, E64, T66, L67, H68, V70.

Thus, as the oxidation degree on the GO surface increases going from G_0 to G_100, the extent of the interaction with the protein also increases. Since an increase in the degree of oxidation of the graphene oxide increases the negatively charged oxygen bearing functional moieties on its surface, which interact with the residues located at the positively charged surface of human ubiquitin through electrostatic interactions, more residues interact with the G_100 than with other GO samples.

Furthermore, the different GO samples did not show any preferential binding to the C or N-terminal part of the protein but the whole amino acid sequence of the protein was seen to be affected. Upon mapping these residues (involved in the interaction with the different GO samples) on the structure of ubiquitin, we found that the beta strands are more affected than the alpha helices of the protein (Fig. 5). We have mapped these residues undergoing a significant reduction (≥75%) in T_2 (^1H_N) values on the electrostatic surface of ubiquitin. We found that these residues are located towards the positively charged surface of ubiquitin (Fig. 6).

The interaction of negatively charged functional moieties on the GO surface with the positively charged surface of ubiquitin is electrostatically favoured. For obtaining the surface plots as shown in Fig. 6, we have used implicit solvent methods to calculate the electrostatic potential on the protein structure considering the solvent to be a dielectric continuum and using the APBS (Adaptive Poisson–Boltzmann Solver) in PYMOL together with a web-based service provided[39,42] at http://www.poissonboltzmann.org/. This further supports the hypothesis that the protein–GO interaction is largely electrostatic in nature and the interacting residues lie on the positively charged surface of the protein.

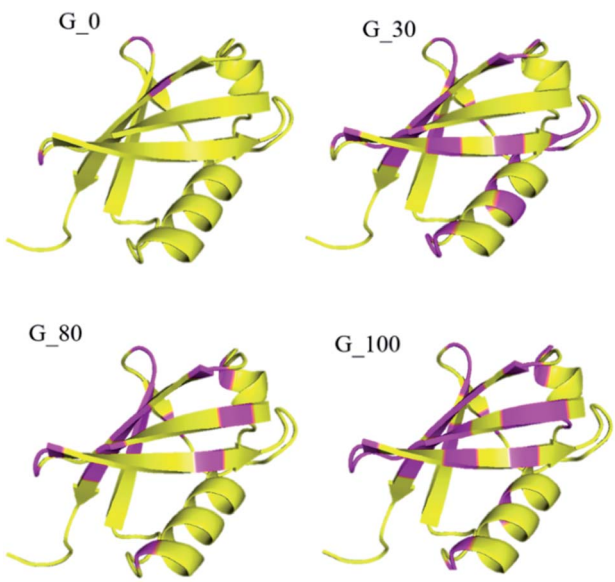

Fig. 5 Mapping the residues on the surface of the ubiquitin involved in the interaction with various GO samples. The preferential binding sites of the different GO samples with the beta strands compared to the helices are highlighted in pink on the structure of ubiquitin.

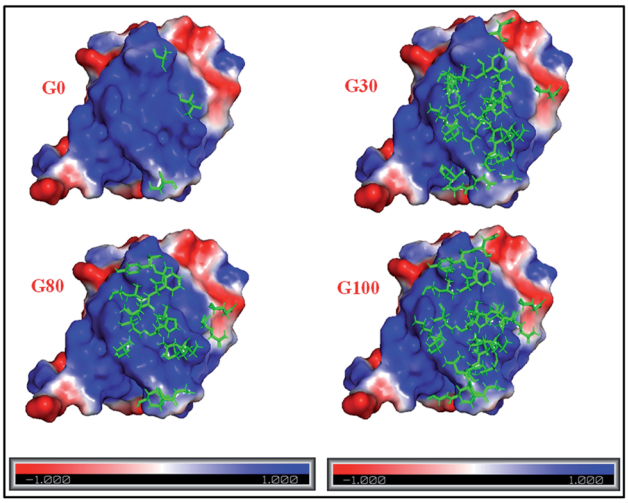

Fig. 6 Electrostatic surface potential of human ubiquitin. The red and blue coloured areas correspond to negatively and positively charged areas, respectively; residues marked in green represent the protein backbone residues (shown in Fig. 5) involved in the interaction with different GO samples.

Reverse titration of ubiquitin with various GO samples

In this titration, ^{15}N-labeled ubiquitin (stock concentration 500 μM) was gradually added to 500 μl of each GO sample (70 μg ml^{-1}) present in the NMR tube. Carrying out reverse titration has two benefits: First, reverse titration helps to verify that the protein bound to the GO surface forms a high molecular weight conjugate having a very short T_2 and hence is invisible to NMR as such. We have taken 70 μg ml^{-1} of each GO sample (500 μl) in a 5 mm NMR tube and the protein was gradually added to the GO. The first few additions of protein to the GO did not show peaks in the HSQC spectra, and hence a control experiment was carried out where the same concentration of ubiquitin was added to the same volume of buffer in the absence of GO. The protein at this concentration yielded a spectrum with the all the cross peaks present. This rules out the possibility that the absence of the peaks in the GO containing sample is due to the lower sensitivity of the protein at this concentration (as shown in Fig. S7 in the ESI†). This implies that in case of GO containing samples the absence of the signal can be attributed to a major population of ubiquitin bound to the GO surface, which is present in excess compared to the free protein in the initial stages of the titration. Even at a relatively higher protein concentration (~35.7 μM), weak signal intensities were observed in the protein-GO conjugates (Fig. S7†). The subsequent additions of the protein led to an increase in the intensities of the cross peaks and more and more peaks showed up in the spectrum. Secondly, for different GO samples bearing different surface chemistries, the amount of bound protein also

varies, as calculated theoretically from the reverse titration (as described in the ESI†).[25,37]

1 μg of G_0 binds ~3 μg of Ubq
1 μg of G_30 binds ~5.7 μg of Ubq
1 μg of G_80 binds ~4.3 μg of Ubq
1 μg of G_100 binds ~5.7 μg of Ubq

The difference in the loading capacity of the different GO samples is confirmed by the BCA assay.[43] This variable loading capacity of different GO samples is dependent upon their surface charge which in turn depends on the degree of oxidation.

Discussion

In recent decades, many studies have been carried out to understand the underlying mechanism of the protein–nanomaterial interactions which remain the crucial step in therapeutic applications of GO-based nanomaterials.[44,45] The binding of GO with biomolecules may involve electrostatic, hydrophobic, covalent and non-covalent, hydrogen bonding, and π–π stacking interactions depending upon the surface charge, energy and hydrophobicity of the interacting partners. It is a well-known fact that the degree of oxidation of GO has a significant role to play in its drug-loading efficiency, the stability of the loaded drug, and also the release of the drug from the GO surface.[46] The higher degrees of oxidation of GO are related to its highly toxic nature under *in vivo* conditions.[47] The toxicity of graphene oxide depends upon the type of functional groups at the surface and the extent of the degree of the oxidation.[12] The effects of graphene-based materials on different globular proteins like lysozyme, trypsin, bovine haemoglobin and ubiquitin have been studied. It has been shown that proteins may undergo a conformational change upon interaction with these graphene-based materials. Yitong B. *et al.*, using Th-T, UV-Vis and CD spectroscopy, showed that exposure to GO induces severe secondary conformational changes in lysozyme and hence the loss of enzymatic activity in lysozyme was observed.[48] G. Fang *et al.* utilized NMR spectroscopy and observed that Graphene Quantum Dots (GQDs) have the potential to interact with the hydrophobic residues of ubiquitin and reduce the beta sheet content of ubiquitin.[49] In another study Yanqing Wang *et al.* studied the effect of GO on the secondary structure of bovine haemoglobin (BHb). The interactions were found to be non-covalent including hydrophobic, van der Waals, hydrogen bonding, and electrostatic interactions. These studies suggested that there is a decrease in the thermal stability and loss of the protein secondary structure upon interaction with GO. In another study, interactions of GO with human serum albumin (HSA) were found to increase at lower pH, and above the isoelectric point of the protein, the interactions were found to decrease because of the electrostatic nature.[50] Thus, it seems that electrostatic interactions are majorly involved in protein and GO binding. These interactions are weak in nature, and so a dynamic exchange of the proteins on the surface of GO is expected.[25]

In our studies, we have used solution sate NMR spectroscopy as a principal technique to probe the underlying mechanism of the interaction of human ubiquitin (at the individual residue level) with GO having different degrees of oxidation. Our results suggest that the extent of interaction of human ubiquitin with the negatively charged surface of GO depends on the degree of oxidation. The interacting residues are found to be located on the beta strands of the protein structure at the positively charged surface of ubiquitin. Thus, the interaction between human ubiquitin and different GO samples having different defect densities and oxidation degrees at a pH of 6 is electrostatic in nature (the pI of ubiquitin is ~6.8). Upon binding, human ubiquitin does not show any change in the chemical shift of the peaks in the 2D [^{15}N–^{1}H] HSQC spectrum which shows that there is no secondary structure change in the protein upon binding which is supported by CD spectroscopy (Fig. S5 in the ESI†). Moreover, we found that binding to the different GO samples leads to a decrease in the T_2 ($^{1}H_N$) values of the protein, and also the K_d falls in the micromolar range, and hence a weak interaction between interacting partners is seen. Thus, a fast-dynamic exchange of the protein molecules on the surface of each GO sample with the free protein molecules in the solution is observed. Also the reverse titration shows that the amount of the protein loaded on the GO surface is a function of the degree of oxidation and the surface charge of both the interacting partners.

Conclusions

In summary, ubiquitin (a globular protein) interacts electrostatically with graphene oxide having varying degrees of oxidation and undergoes a dynamic and reversible exchange (fast exchange regime) from the surface of the GO as revealed by NMR relaxation studies and ITC. The interaction does not involve any change in the secondary structure of the protein. This study helps in understanding the mechanism of the interaction of a globular protein with graphene-based nanomaterials with different defect densities and surface chemistry and thus will help in designing appropriate graphenic materials for use in various biomedical fields like drug delivery, biomedical devices and imaging.

Conflicts of interest

There are no conflicts to declare.

Acknowledgements

The authors would like to acknowledge the NMR Research Centre at IISc Bangalore, Department of Science and Technology (DST) (IR/S0/LU-007/2010) and the University Grants Commission (UGC), India for the financial support. The Departments of the Centre for Nano Science and Engineering and MBU are highly acknowledged for their help in recording the Raman spectra and ITC data, respectively.

Notes and references

1 C. Chen, S. Rosenblatt, K. I. Bolotin, W. Kalb, P. Kim, I. Kymissis, H. L. Stormer, T. F. Heinz and J. Hone, *Nat. Nanotechnol.*, 2009, **4**, 861–867.

2 T. Shimizu, J. Haruyama, D. C. Marcano, D. V. Kosinkin, J. M. Tour, K. Hirose and K. Suenaga, *Nat. Nanotechnol.*, 2011, **6**, 45–50.
3 F. Léonard and A. A. Talin, *Nat. Nanotechnol.*, 2011, **6**, 773–783.
4 C. N. R. Rao, H. S. S. R. Matte and K. S. Subrahmanyam, *Acc. Chem. Res.*, 2013, **46**, 149–159.
5 L. Vicarelli, S. J. Heerema, C. Dekker and H. W. Zandbergen, *ACS Nano*, 2015, **9**, 3428–3435.
6 D. Chen, H. Feng and J. Li, *Chem. Rev.*, 2012, **112**, 6027–6053.
7 C. Chung, Y. Kim, D. Shin, S. Ryoo, B. H. E. E. Hong and D. Min, *Acc. Chem. Res.*, 2013, 2211–2224.
8 L. Feng, L. Wu and X. Qu, *Adv. Mater.*, 2013, **25**, 168–186.
9 V. Georgakilas, J. N. Tiwari, K. C. Kemp, J. A. Perman, A. B. Bourlinos, K. S. Kim and R. Zboril, *Chem. Rev.*, 2016, **116**, 5464–5519.
10 D. C. Marcano, D. V. Kosynkin, J. M. Berlin, A. Sinitskii, Z. Sun, A. Slesarev, L. B. Alemany, W. Lu and J. M. Tour, *ACS Nano*, 2010, **4**, 4806–4814.
11 D. W. Lee, L. V. De Los Santos, J. W. Seo, L. L. Felix, A. D. Bustamante, J. M. Cole and C. H. W. Barnes, *J. Phys. Chem. B*, 2010, **114**, 5723–5728.
12 S. A. Sydlik, S. Jhunjhunwala, M. J. Webber, D. G. Anderson and R. Langer, *ACS Nano*, 2015, **9**, 3866–3874.
13 D. R. Dreyer, S. Park, C. W. Bielawski and R. S. Ruoff, *Chem. Soc. Rev.*, 2010, **39**, 228–240.
14 H. Lai, F. Xu, Y. Zhang and L. Wang, *J. Mater. Chem. B*, 2018, **6**, 4008–4028.
15 C. H. Lu, H. H. Yang, C. L. Zhu, X. Chen and G. N. Chen, *Angew. Chem., Int. Ed.*, 2009, **48**, 4785–4787.
16 J. Balapanuru, J. X. Yang, S. Xiao, Q. Bao, M. Jahan, L. Polavarapu, J. Wei, Q. H. Xu and K. P. Loh, *Angew. Chem., Int. Ed.*, 2010, **49**, 6549–6553.
17 Z. Liu, J. T. Robinson, X. Sun and H. Dai, *J. Am. Chem. Soc.*, 2008, **130**, 10876–10877.
18 Q. Liu, L. Wei, J. Wang, F. Peng, D. Luo, R. Cui, Y. Niu, X. Qin, Y. Liu, H. Sun, J. Yang and Y. Li, *Nanoscale*, 2012, **4**, 7084–7089.
19 D. Jaque, L. Martínez Maestro, B. Del Rosal, P. Haro-Gonzalez, A. Benayas, J. L. Plaza, E. Martín Rodríguez and J. García Solé, *Nanoscale*, 2014, **6**, 9494–9530.
20 T. R. Nayak, H. Andersen, V. S. Makam, C. Khaw, S. Bae, X. Xu, P. L. R. Ee, J. H. Ahn, B. H. Hong, G. Pastorin and B. Özyilmaz, *ACS Nano*, 2011, **5**, 4670–4678.
21 W. C. Lee, C. H. Y. X. Lim, H. Shi, L. A. L. Tang, Y. Wang, C. T. Lim and K. P. Loh, *ACS Nano*, 2011, **5**, 7334–7341.
22 J. Wang, *Chem. Rev.*, 2008, **108**, 814–825.
23 Y. He, B. Jiao and H. Tang, *RSC Adv.*, 2014, **4**, 18294–18300.
24 L. Wu, L. Zeng and X. Jiang, *J. Am. Chem. Soc.*, 2015, **137**, 10052–10055.
25 S. Mondal, R. Thirupathi, P. Rao and H. S. Atreya, *RSC Adv.*, 2016, 52539–52548.
26 Y. Zhang, C. Wu and J. Zhang, *Nanotechnol. Rev.*, 2013, **2**, 27–45.
27 X. Liu, C. Yan and K. L. Chen, *Environ. Sci. Technol.*, 2019, **53**, 8631–8639.
28 K. Yao, P. Tan, Y. Luo, L. Feng, L. Xu, Z. Liu, Y. Li and R. Peng, *ACS Appl. Mater. Interfaces*, 2015, **7**, 12270–12277.
29 Kenry, K. P. Loh and C. T. Lim, *Nanoscale*, 2016, **8**, 9425–9441.
30 B. Sun, Y. Zhang, W. Chen, K. Wang and L. Zhu, *Environ. Sci. Technol.*, 2018, **52**, 7212–7219.
31 F. B. Bombelli, D. Walczyk, M. Monopoli, I. Lynch and K. A. Dawson, *Eur. Cells Mater.*, 2010, **20**, 10.
32 M. Mahmoudi, I. Lynch, M. R. Ejtehadi, M. P. Monopoli, F. B. Bombelli and S. Laurent, *Chem. Rev.*, 2011, **111**, 5610–5637.
33 X. Q. Wei, L. Y. Hao, X. R. Shao, Q. Zhang, X. Q. Jia, Z. R. Zhang, Y. F. Lin and Q. Peng, *ACS Appl. Mater. Interfaces*, 2015, **7**, 13367–13374.
34 F. Emadi, A. Amini, A. Gholami and Y. Ghasemi, *Sci. Rep.*, 2017, **7**, 1–13.
35 A. Ceccon, V. Tugarinov, A. Bax and G. M. Clore, *J. Am. Chem. Soc.*, 2016, **138**, 5789–5792.
36 Z. Mohanta, H. S. Atreya and C. Srivastava, *Sci. Rep.*, 2018, 1–6.
37 S. A. Malik, S. Mondal and H. S. Atreya, *RSC Adv.*, 2019, **9**, 28746–28753.
38 P. K. Mandal and A. Majumdar, *Concepts Magn. Reson., Part A*, 2004, **20**, 1–23.
39 V. P. Brahmkhatri, K. Chandra, A. Dubey and H. S. Atreya, *Nanoscale*, 2015, **7**, 12921–12931.
40 I. Pal, V. P. Brahmkhatri, S. Bera, D. Bhattacharyya, Y. Quirishi, A. Bhunia and H. S. Atreya, *J. Colloid Interface Sci.*, 2016, **483**, 385–393.
41 J. Iwahara, C. Tang and G. Marius Clore, *J. Magn. Reson.*, 2007, **184**, 185–195.
42 L. Calzolai, F. Franchini, D. Gilliland and F. Rossi, *Nano Lett.*, 2010, **10**, 3101–3105.
43 P. K. Smith, R. I. Krohn, G. T. Hermanson, A. K. Mallia, F. H. Gartner, M. D. Provenzano, E. K. Fujimoto, N. M. Goeke, B. J. Olson and D. C. Klenk, *Anal. Biochem.*, 1985, **150**, 76–85.
44 S. S. Chou, M. De, J. Luo, V. M. Rotello, J. Huang and V. P. Dravid, *J. Am. Chem. Soc.*, 2012, **134**, 16725–16733.
45 D. Kim, J. M. Yoo, H. Hwang, J. Lee, S. H. Lee, S. P. Yun, M. J. Park, M. Lee, S. Choi, S. H. Kwon, S. Lee, S. Kwon, S. Kim, Y. J. Park, M. Kinoshita, Y. Lee, S. Shin, S. R. Paik, S. J. Lee, S. Lee, B. H. Hong and H. S. Ko, *Nat. Nanotechnol.*, 2018, **13**, 812–818.
46 C. W. Liu, F. Xiong, H. Z. Jia, X. L. Wang, H. Cheng, Y. H. Sun, X. Z. Zhang, R. X. Zhuo and J. Feng, *Biomacromolecules*, 2013, **14**, 358–366.
47 M. C. Duch, G. R. S. Budinger, Y. T. Liang, S. Soberanes, D. Urich, S. E. Chiarella, L. A. Campochiaro, A. Gonzalez, N. S. Chandel, M. C. Hersam and G. M. Mutlu, *Nano Lett.*, 2011, **11**, 5201–5207.
48 Y. Bai, Z. Ming, Y. Cao, S. Feng, H. Yang, L. Chen and S. T. Yang, *Colloids Surf., B*, 2017, **154**, 96–103.
49 G. Fang, B. Luan, C. Ge, Y. Chong, X. Dong, J. Guo, C. Tang and R. Zhou, *Carbon*, 2017, **121**, 285–291.
50 Y. Wang, Z. Zhu, H. Zhang, J. Chen and B. Tang, *Mater. Chem. Phys.*, 2016, **182**, 272–279.